Nuclear Materials and Energy 15 (2018) 103–109

Contents lists available at ScienceDirect

Nuclear Materials and Energy

journal homepage: www.elsevier.com/locate/nme

Stress corrosion cracking susceptibility of 310S stainless steel in hydrogenated hot water

Yen-Jui Huang[a,*], Kousuke Kawakita[a], Akihiko Kimura[b]

[a] Graduate School of Energy Science, Kyoto University, Uji, Kyoto, Japan
[b] Institute of Advanced Energy, Kyoto University, Uji, Kyoto, Japan

ARTICLE INFO

Keywords:
SSRT
Hydrogen assisted SCC
Cross slip
Stacking fault energy

ABSTRACT

The stress corrosion cracking (SCC) susceptibility of solution-annealed 310S stainless steel (SS) was examined by means of slow-strain rate test (SSRT) method in hot water (288 °C) with dissolved-hydrogen (DH), and the results were compared with those of 316L SS. Almost no SCC was observed in 310S SS, while a remarkable SCC was found in 316L SS showing brittle fracture surfaces and cracks on specimen side surfaces. The SCC observed in 316L SS started as IGSCC while necking, and transferred to TGSCC. It was also shown that sensitization resulted in the suppression of IGSCC of 316L SS. On the assumption that the SCC in hydrogenated hot water can be interpreted in terms of hydrogen assisted SCC, the mechanism of the suppression of SCC in 310S SS is related with a higher nickel content which increases stacking fault energy and facilitates cross slip of dislocations, resulting in the reduction of hydrogen concentration on a unit area of slip plane.

1. Introduction

The water-cooled ceramic breeder testing blanket module (TBM) is one of key components of International Thermonuclear Experimental Reactor and beyond towards nuclear fusion energy. In the design of the TBM, a reduced activation ferritic/martensitic steel has been selected as structural material cooled by water similar to the current pressurized water reactors (PWR). Behind the TBM there is a primary heat transfer system that is responsible for heat exchange and tritium recovery where long cooling pipes made of 316L stainless steel (SS) are installed [1–6]. In the blankets, tritium, a fuel of fusion reactor, is produced through nuclear reactions and it could penetrate into cooling water. With the aid of radiation, tritium (T) may react with water and forms tritiated water (such as THO or T_2O) and/or TH, T_2 as dissolved gaseous species in the coolant.

Regarding the effect of dissolved hydrogen on stress corrosion cracking (SCC), current PWRs adopt hydrogen injection to reduce corrosion potential for scavenging corrodants for maintaining structural integrity. The content of dissolved-H_2 (DH) is a key and should be kept within a certain range to maximize efficiency while not degrading materials. In order to investigate the effect of hydrogen on SCC, a number of studies were performed by means of slow strain rate test (SSRT) and compact tension (CT) test with focusing on the measurement of crack growth rate (CGR) of solution annealed and/or cold worked SS in simulated PWR primary loop water.

Arioka conducted SSRT on solution-annealed 316 SS at different temperatures and found a minimum CGR at 15 cc H_2/kg H_2O in the temperature range of 320–340 °C and at around 25 cc H_2/kg H_2O at 310 °C [7]. On cold-worked 316L SS, Fukumura et al. [8] reported a monotonic increase from 15 to 45 cc H_2/kg H_2O at 320 °C, which is supported by Choi et al. tested at 340 °C [9]. However, Meng et al. found a monotonic CGR decrease from 0 to 50 cc H_2/kg H_2O [10]. Nonetheless, Zhong et al. found a CGR peak at 15 cc H_2/kg H_2O at 325 °C [11]. Raquet et al. reported a CGR peak at 30 cc H_2/kg H_2O at 360 °C on V-shape humped 304L SS [12]. As shown above, although the effect of hydrogen content is not clear, it is considered that hydrogen play two roles in suppression of formation of protective film thickness [13] and in reduction of atomic bond strength of which the balance determines the total effect of hydrogen on SCC.

The fracture mode of SCC in the water dissolved with hydrogen is also different among the researchers; transgranular (TG), intergranular (IG) or mix mode. Meng et al. [10] and Chen et al. [14] revealed IGSCC for a cold-worked 316NG tested in the water with DH 2.5 ppm at 310 °C. Nono et al. [15], however, reported TGSCC on solution-annealed 316L SS in the water with DH = 0.4 ppm at 288 °C. Arioka [7] found that crack initiated in IG mode and transformed into TG mode in the water with 30 cc H_2/kg H_2O at 320 °C. As for nickel base alloys, several researchers reported that CGR showed a peak [7,8,11] or increased [10] with hydrogen contentment. These above mentioned experimental results suggests that hydrogen effect also depends on

* Corresponding author.
E-mail address: y-huang@iae.kyoto-u.ac.jp (Y.-J. Huang).

https://doi.org/10.1016/j.nme.2018.03.004
Received 15 December 2017; Received in revised form 12 February 2018; Accepted 9 March 2018
Available online 22 March 2018

material even for iron based austenitic SS.

Austenitic SS also suffer hydrogen embrittlement in a dry hydrogen gas. Caskey [16] carried out tensile tests at temperature ranging from 77–373 K for several iron-based austenitic stainless steels charged with deuterium in a deuterium atmosphere (D_2) at 69 MPa, and he found that the susceptibility to hydrogen embrittlement of 310S SS is much less than 304L SS at around 200 K. He also indicated that, in Fe–Cr–Ni ternary alloy system, the susceptibility reduced as Ni content was as high as within 15–25 wt%. Han et al. [17] reported the similar results with him. After the hydrogen or deuterium charging in 1 MPa of H_2 and D_2 gas, Zhang et al. [18] tested several types of 316 SS with various Ni content and showed that the susceptibility was reduced with Ni equivalent content of the austenitic steel.

We consider that 310S SS is more resistant to SCC under HT/T_2-dissolved hot water because 310S SS may behave in a similar manner in tritiated water as in hydrogen gaseous environment. In this research, the SCC susceptibility of solution-annealed 310S SS, which is rather highly resistant to hydrogen embrittlement, was examined by means of SSRT in hot water with dissolved-hydrogen and the results are compared with that of 316L SS. Furthermore, the effects of sensitization treatment on the SCC in hydrogenated water was investigated.

2. Experimental

2.1. Materials

The materials used in this study were commercial plate type 316L SS and 310S SS. Their chemical compositions were listed in Table 1. The geometry of tensile specimens is shown in Fig. 1, of which the gage section measures 5 mm in length, 1.2 mm in width and 0.5 mm in thickness. All the specimens were solution-annealed at 1050 °C for 1 h, followed by quenching into iced water. A part of these tensile specimens were further heat-treated at 700 °C for 100 h followed by water quench so as to simulate sensitization caused by post-weld heat treatment after welding. Specimen surface was polished from #1200 to #4000 with SiC sand papers then buff-polished to 0.25 μm with diamond pastes. After polishing, the specimens were cleaned in ultrasonic cleaner with demineralized water. The grain microstructure of solution-annealed specimens were shown in Fig. 2 after the etching in a solution mixed 10 g oxalic acid with 100 ml demineralized water. The averaged grain sizes were measured by means of intersection method and they were 26 and 59 μm for 310S and 316L SS, respectively.

2.2. Hot water loop for SSRT

The hot water circulation loop includes a primary loop and a water chemistry monitoring loop, as shown in Fig. 3. The high purity nitrogen and hydrogen were injected into a water tank to control dissolved-oxygen (DO) and dissolved-hydrogen (DH) content. A high pressure pump sent high purity water into a heat exchanger, pre-heater then to the autoclave where a SSRT specimen was set. The hot water is chilled through another heat exchanger and then back to the water tank. SSRT was conducted in the autoclave at a strain rate of 5×10^{-7}/s. Testing temperature and pressure was kept at 288 °C and 7.8 MPa with conductivity kept below 0.1 μS/cm. Two different water conditions were chosen for SSRT: one was of water dissolved with 1.4 ppm of hydrogen (DH = 1.4 ppm) and the other was of deaerated condition (both DO and DH < 0.01 ppm).

Table 1
Chemical compositions of 316L and 310S SS.

wt%	C	Si	P	S	Cr	Ni	Mo	Mn	Co	Fe
310S SS	0.02	0.7	0.022	–	24.76	19.17	–	0.8	0.1	bal.
316 L SS	0.01	0.73	0.032	0.004	17.41	12.13	2.05	1.06	–	bal.

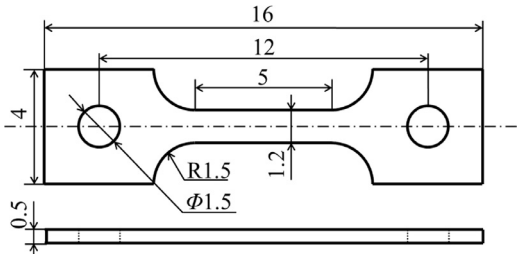

Fig. 1. The geometries of miniaturized specimens for SSRT.

After SSRT, fracture surface and side surface were observed by a scanning electron microscope (SEM). The fracture mode of crack initiation was examined by electron backscattering diffraction (EBSD) method with the orientation imaging microscopy (OIM) detector equipped in a field-emission type SEM (Ultra-55, Carl Zeiss Co., Ltd.).

3. Results

3.1. Stress–strain behavior

Fig. 4 shows the stress-strain curves of solution-annealed (SA) 316L and 310S SS under deaerated and DH = 1.4 ppm hot water condition. Solid lines represent deaerated water condition and dashed lines represent DH = 1.4 ppm water condition. The ultimate tensile strength (UTS) and total elongation (TE) of 310S SS are larger than those of 316L SS. Although the difference is not significant, it appears that the total elongation is smaller in the case of DH = 1.4 ppm water condition than deaerated water condition. A similar trend was observed for sensitized specimens, as shown in Fig. 5, where the stress-strain curves of sensitized (SEN) 316L and 310S SS were shown. The presence of dissolved-hydrogen again reduced the total elongation of 316L and 310S SS. In other words, the dissolved-hydrogen decreases total elongation irrespective of heat treatment conditions. Comparing the total elongations of both steels between SA and SEN, no remarkable difference was observed between two conditions in the water deaerated and DH = 1.4 ppm. The stress-strain behavior will be discussed again more in detail after showing fracture behavior.

3.2. Fracture behavior

The fractography of fractured surface and side surface is summarized in Fig. 6 for SA 316L SS/SA 310S SS under (a)/(c) deaerated and (b)/(d) DH 1.4 ppm water condition, respectively. In each column, the top represents the overview of fracture surface; the middle represents the enlarged area squared with white broken line; and the bottom represents side surface near fractured surface. Although the stress-strain behaviors in Fig. 5 are almost same among the specimens, the fracture mode is significantly influenced by experimental conditions, such as material and water chemistry. It is obvious that the fracture mode of 310S SS is almost completely ductile, while that of 316L SS is mostly brittle. The brittle fracture mode of 316L SS is mainly transgranular type, exhibiting river patterns, that is, TGSCC. A number of large cracks are also found on the side surfaces of 316L SS, while small cracks appear to be formed on 310S SS. It can be said that 310S SS is more resistant to occurrence of TGSCC than 316L SS. On the enlarged view of fractured surface of 316L SS under deaerated and DH 1.4 ppm (Fig. 6(a) and (b)) condition and of 310S SS under deaerated condition (Fig. 6(c)), some cracks appear to initiate with IGSCC and propagate as TGSCC with typical river-patterns in 316L SS. But, in 310S SS under DH 1.4 ppm (Fig. 6(d)), fine wavy crack patterns are also found. The cross sectional view was observed for the fractured specimens using SEM-EBSD and the results are shown in Fig. 7, indicating that the fracture mode of crack initiation of SA 316L and SA 310S SS under DH 1.4 ppm condition is intergranular. However, it is noted that most of crack

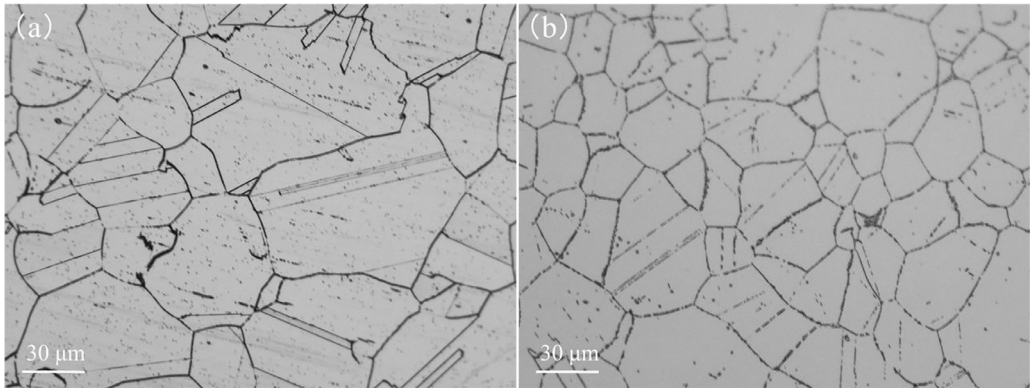

Fig. 2. The microstructures of solution-annealed (a) 316L and (b) 310S SS.

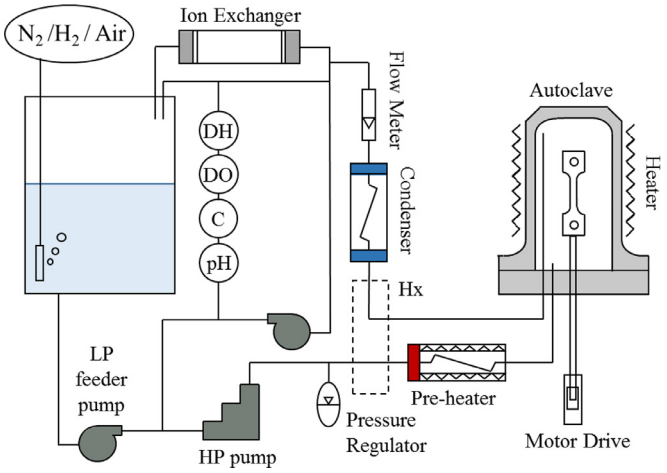

Fig. 3. Schematic view of SSRT loop used in this work.

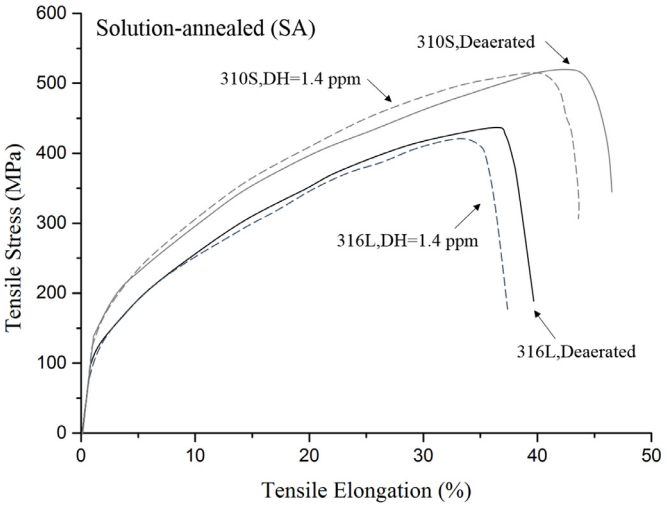

Fig. 4. Stress–strain curves of solution-annealed (SA) 316L and 310S SS tested in hot water (288 °C, 7.8 MPa) at deaerated condition (solid line) and with DH = 1.4 ppm (dash line).

initiation sites in SEN steels is transgranular type. Accordingly, it is considered that both the solution-annealed steels suffer embrittlement initiating as IGSCC at specimen surface and the cracks mostly penetrate into grains as TGSCC showing river patterns on the fractured surfaces, though the susceptibility to SCC is much lower in 310S SS than 316L SS.

A similar trend but smaller effects were observed for sensitized specimens. The fractography of fractured surface and side surface of SEN 316L SS/SEN 310S SS under (a)/(c) deaerated and (b)/(d) DH

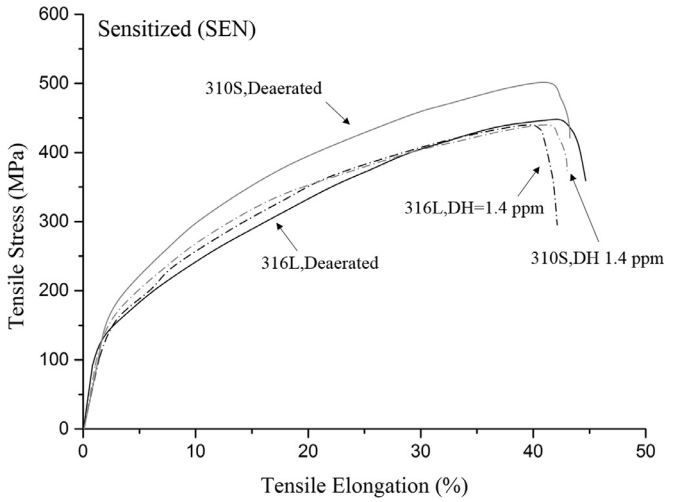

Fig. 5. Stress–strain curves of sensitized (SEN) 316L and 310S SS tested in hot water (288 °C, 7.8 MPa) at deaerated condition (solid line) and with DH = 1.4 ppm (dash line).

1.4 ppm water condition is summarized in Fig. 8. In 316L SS, the brittle fracture ratio (BFR) of DH 1.4 ppm condition is smaller than that of deaerated condition, and in both the conditions cracks initiates and propagates as TGSCC. In 310S SS, the brittle fracture and cracks on side surface are almost unseen under two water conditions. These suggest that the susceptibility to SCC in hydrogenated water is reduced by sensitization treatment in both steels.

4. Discussion

4.1. Experimental conditions

In this research, we examined SCC susceptibility by SSRT method with use of rather small specimens. Compact tension (CT) test with pre-cracked specimens is suitable for crack growth rate measurement under an applied stress intensity factor, while SSRT is a convenient test method to investigate crack initiation process under increasing applied stress, which is accompanied by cold work. It has been proved by tests with CT specimens that crack growth rates of prior-deformed 304L SS and 316NG SS as well as 316L HAZ and 316NG weld metal in high temperature water decreased significantly after introducing hydrogen gas in to solution [19–22]. Thus, it was clearly shown by CT tests that hydrogen suppressed crack growth rate of IGSCC in water with dissolved oxygen. We focused on the SCC susceptibility difference through the investigation of the effect of dissolved hydrogen on the initiation of SCC by means of SSRT method.

As well known, utilization of miniaturized tensile specimens, especially thin specimens, sometime resulted in the change in the fracture

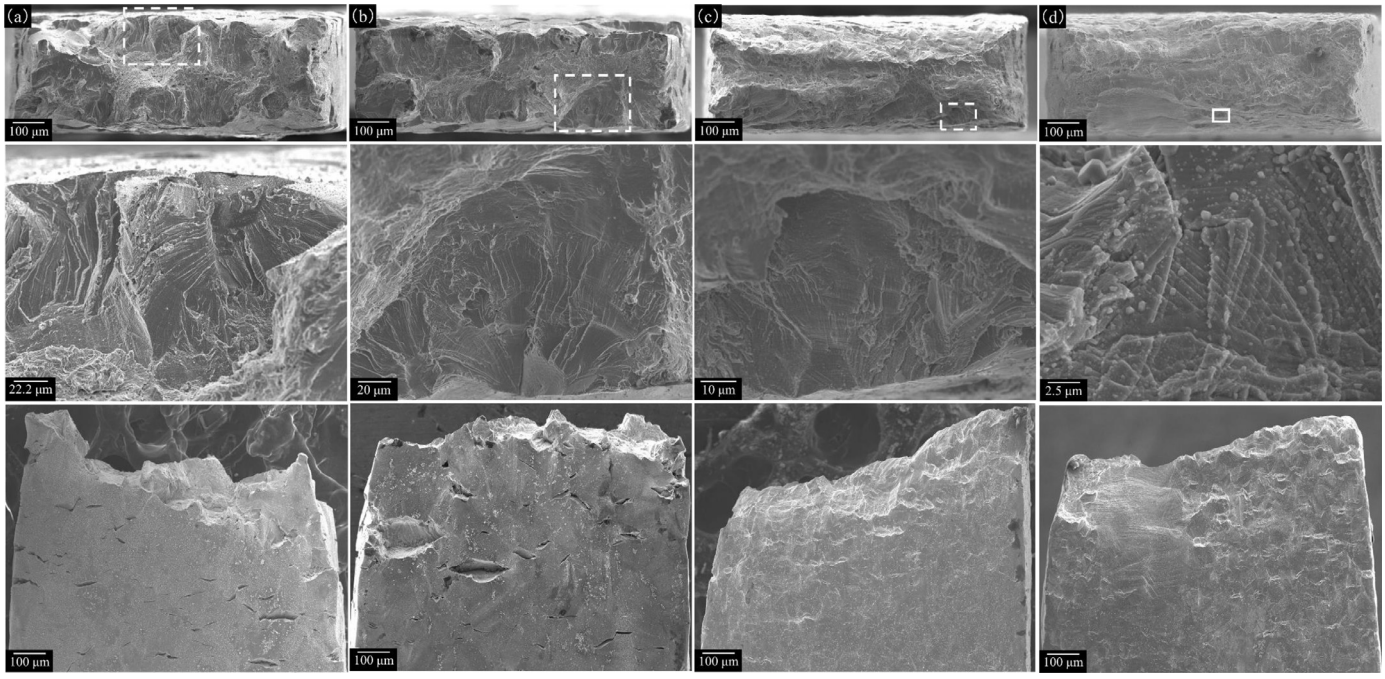

Fig. 6. SEM photos of solution-annealed 316L SS under (a) deaerated and (b) DH 1.4 ppm water condition; and 310S SS under (c) deaerated and (d) DH 1.4 ppm water condition. In each column, from top to bottom represents the overview of fracture surface, the enlarged area squared with white line and the side surface near fractured surface.

mode because of the alternation in stress state. However, in our previous research, the specimen thickness of our miniaturized specimens was thick enough to investigate the trend of crack mode change, IG or TG [23,24] Authors believe that the effect of dissolved hydrogen on SCC susceptibility evaluated with present miniaturized specimens can be compared between two steels.

4.2. SCC in hydrogenated hot water

As reported in the previous works on SCC in hydrogenated water, hydrogen injection into hot water often accelerates the CGR of IGSCC and/or TGSCC depending on the amount of dissolved hydrogen [8,9], suggesting that there is an appropriate amount of hydrogen to suppress

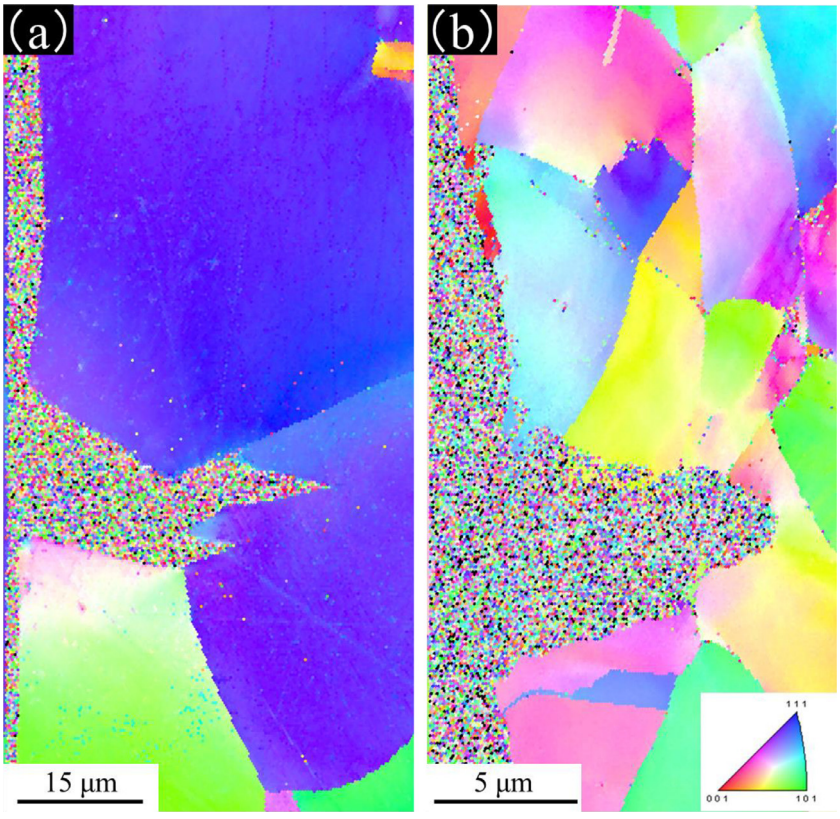

Fig. 7. The crack initiation of solution-annealed (a) 316L and (b) 310S SS under DH 1.4 ppm water condition. In both two materials, intergranular crack forms at the surface then propagates into grains as transgranular cracks.

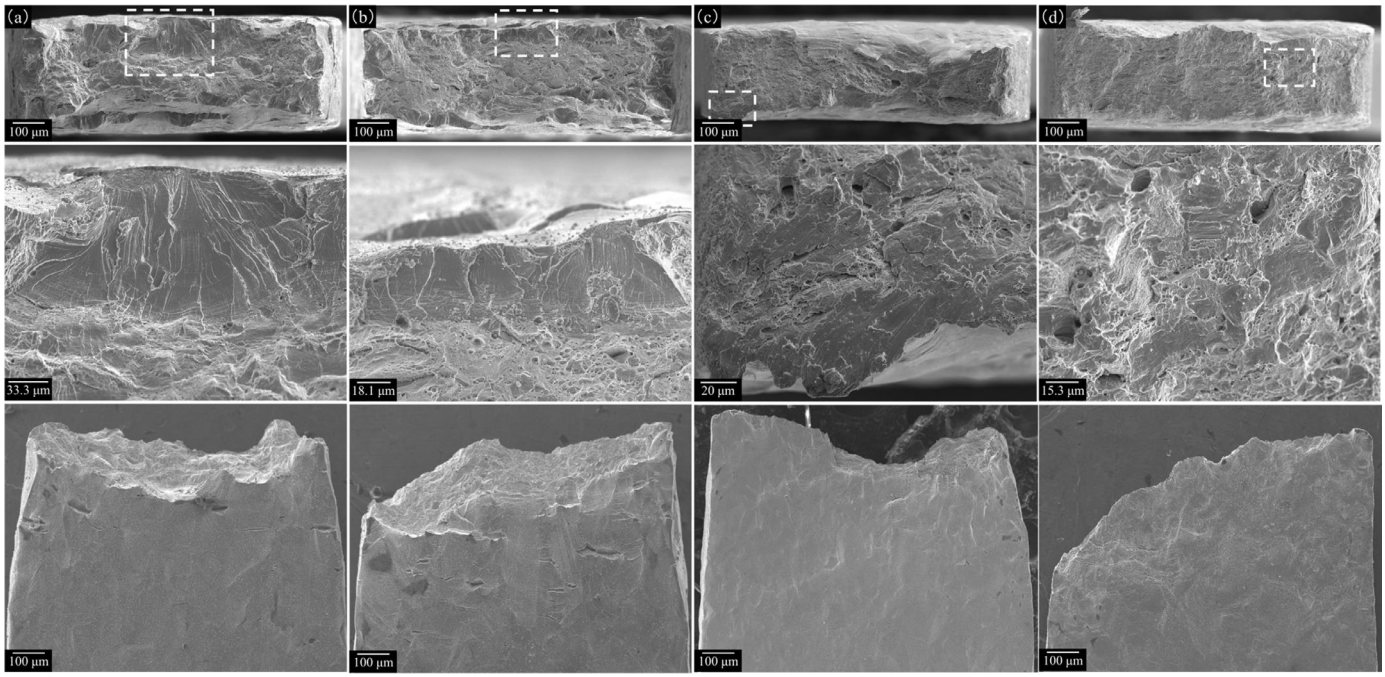

Fig. 8. SEM photos of sensitized 316L SS under (a) deaerated and (b) DH 1.4 ppm water condition; and 310S SS under (c) deaerated and (d) DH 1.4 ppm water condition. In each column, from top to bottom represents the overview of fracture surface, the enlarged area squared with white line and the side surface near fractured surface.

the SCC [7], and the CGR of SCC may show a peak at an amount of dissolved hydrogen [11,12,23,25–28]. With increasing the amount of dissolved hydrogen in hot water, SCC can be accelerated by thickness reduction of protective film but a further increase results in the suppression of SCC caused by reduction of corrosion rate that is accompanied by the reduction of hydrogen production at a crack nucleation site.

Although the acceleration mechanism of SCC with increasing dissolved hydrogen is not clear, in the present study, we try to explain the difference in SCC susceptibility between 316L SS and 310S SS in terms of hydrogen-assisted SCC caused by both the corrosion assisted hydrogen production and the reduction of fracture toughness of the stainless steels.

4.3. Comparison between 310S and 316L SS

The difference in the mechanical properties between 310S and 316L SS is summarized in Fig. 9. As mentioned before, the stress–strain behavior, namely, yield stress (YS), ultimate tensile stress (UTS) and total elongation (TE) are almost not influenced by dissolved hydrogen content. However, the fracture relating properties, reduction area (RA), brittle fracture ratio (BFR), the number of cracks and total length of cracks on the side surfaces of specimens indicates remarkable difference between 310S and 316L SS, where RA is defined as the ratio of final-fractured surface area to original cross-section area, and BFR is defined as the ratio of brittle-fracture mode area to final-fractured surface area. It can be said that regardless the existence of hydrogen, in solution-annealed and sensitized steels, the RA of 310S SS is higher than that of 316L SS, and the BFR of 310S SS is lower than that of 316L SS. At solution-annealed condition, the BFR of 316L SS is over 30%, while of 310S SS is less than 5%; and, at sensitized condition, the BFR of 316L SS is over 20%, while 310S SS is almost ductile. Therefore, comparing the results between 316L SS and 310S SS, the susceptibility to SCC is much lower in 310S SS than 316L SS, which is in a good agreement with that of hydrogen embrittlement [16].

The major difference in the chemical compositions between the two steels are chromium (Cr), nickel (Ni) and molybdenum (Mo)m as shown in Table 1. Among these elements, Ni is well known as an element increasing stacking fault energy (SFE) in steels. [29–32] Since higher the SFE is, the smaller the distance between two partial dislocations, in 310S SS with much higher Ni content, moving dislocations easily cross-slip, which increases the number of active slip planes. Fig. 10 shows the examples of typical slip lines on the specimen side surface of SA 316L and SA 310S SS after SSRT in hot water with DH = 1.4 ppm. The slip lines observed in 316L SS are coarse and straight suggesting that dislocations move on the limited slip planes, while those of 310S SS are fine and wavy that indicates cross-slip occurs frequently and consequently the number of dislocations on a slip plane is small. In Fig. 9, the total length of cracks is larger in 316L SS than 310S SS, while the number of cracks is almost same between the two steels. The averaged distance between slip bands of 316L and 310S SS is measured for Fig. 10 and estimated to be 2.4 and 1.5 μm, respectively, indicating more frequent cross-slip in 310S SS than 316L SS. When the number of active slip plane increases, the number of dislocations on the unit area of slip plane decreases. Since hydrogen is trapped in the dislocation core, the content of hydrogen on the slip plane is reduced with decreasing dislocation density, and consequently hydrogen effect is reduced. It is considered that at deaerated and DH = 1.4 ppm conditions, a lower potential causes suppression of the formation of protective surface oxide film and hydrogen reduces cohesive force of lattice atoms, which results in SCC.

4.4. Effect of sensitization heat treatment

In general, the IGSCC in hot water with dissolved oxygen is enhanced by so-called sensitization treatment which causes Cr depletion at grain boundaries. In this research, however, the IGSCC was suppressed by sensitization in water with dissolved hydrogen. We are focusing on the interpretation of this behavior by hydrogen trapping in hydrogen-assisted SCC.

The microstructure of SEN 316L SS was examined by TEM-EDX line scan, and shown in Fig. 11, indicating that small Cr carbide exists both on grain boundaries and in the grains. The Cr is slightly depleted near the grain boundary, creating a Cr-depleted zone. Since carbides are one of effective trapping sites for hydrogen [33], it is considered that hydrogen transport along grain boundaries and through bulk diffusion

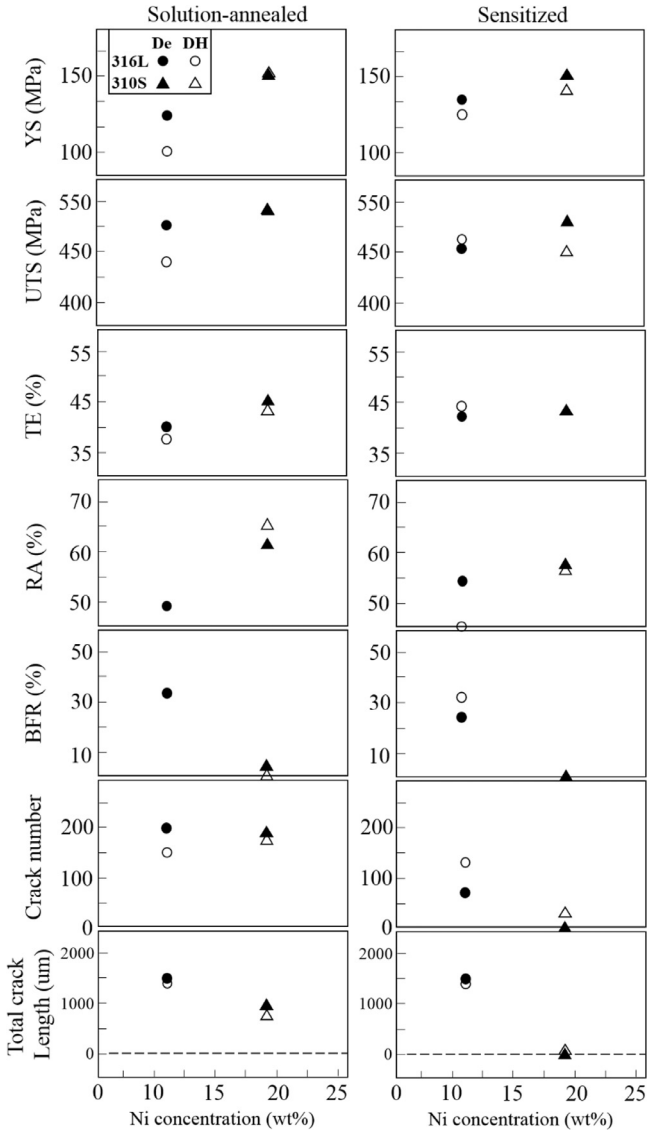

Fig. 9. Mechanical properties of 310S SS and 316L SS after solution annealing and sensitization: YS (yield stress), UTS (ultimate tensile strength), TE (total elongation), RA (reduction of area), BFR (brittle fracture ratio, number of cracks and total crack length) in (left) SA series and (right) SEN series. Circle represents 316L SS while triangle the 310S SS; solid symbol represents deaerated water condition and open symbol the DH 1.4 ppm water condition.

could be suppressed in the sensitized steels. Both the intergranular and transgranular carbides play a role as a strong hydrogen trapping site, and they prevent hydrogen from concentrating at crack nucleation site as grain boundaries and slip planes in the material, then reduce the

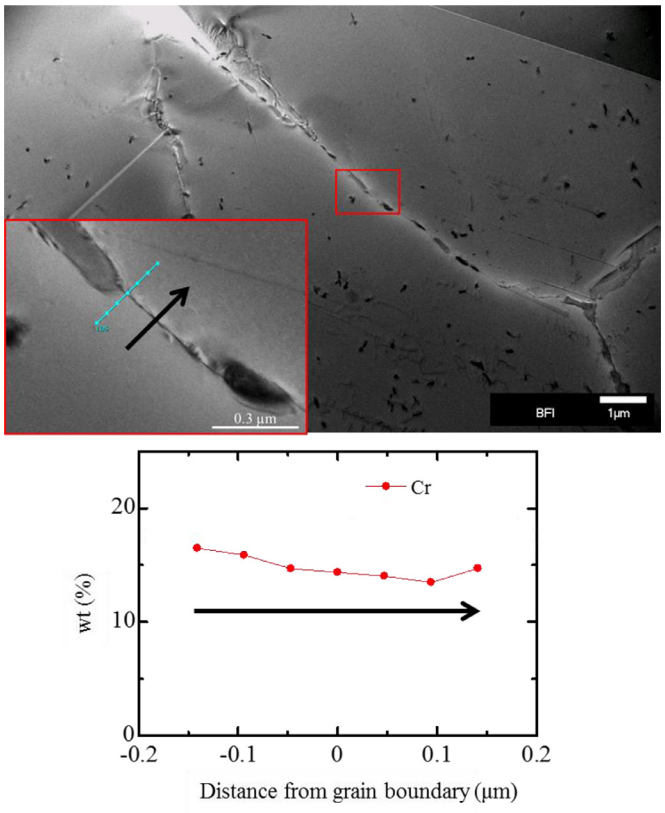

Fig. 11. TEM photo and EDX line scan of SEN 316L SS. Cr content is slightly decreased at around grain boundary.

susceptibility to SCC at the same amount of dissolved hydrogen. This may explain the difference in cracking mode between solution-annealed steels and sensitized steels. In solution-annealed steels, the brittle fracture initiates as IGSCC and propagate into TGSCC, while in sensitized steels, the brittle fracture of 316L SS initiates and propagates as TGSCC. The suppression of IGSCC in sensitized steel might be due to suppression of hydrogen transport along grain boundaries caused by hydrogen trapping at grain boundary carbides.

5. Conclusions

The susceptibility to SCC of 310S and 316L SS in hydrogen-dissolved hot water (both DO and DH < 0.01 ppm and DH = 1.4 ppm) at 288 °C and 7.8 MPa was examined by SSRT at a strain rate of 5×10^{-7}/s. The obtained main results are as follows;

(1) Solution-annealed 310S SS is much more resistant to SCC in hydrogenated water than solution-annealed 316L SS, showing that the BFR of 310S SS is at most 5%, while that of 316L SS is over 30%. In

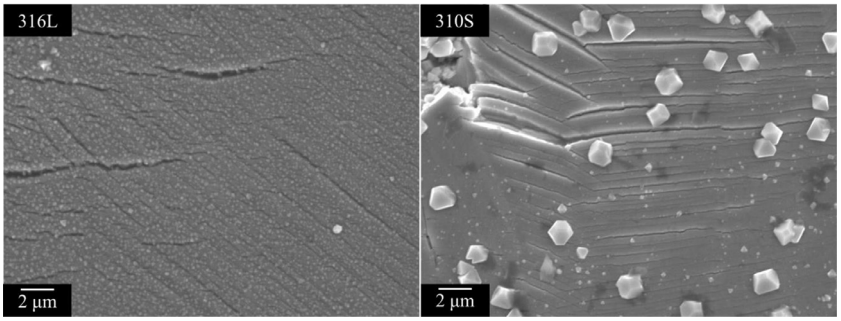

Fig. 10. The slip lines morphology on the specimen surface of (left) SA 316L and (right) SA 310S at dissolved-hydrogen 1.4 ppm condition.

both steels the SCC initiated at grain boundaries and transferred to slip planes in grains.

(2) The slip line morphology observation revealed that the slip lines are fine in 310S SS and coarse in 316L SS. The total length of cracks is larger in 316L SS than 310S SS, while the number of cracks is almost same between the two steels. The averaged distance between slip bands of 316L and 310S SS is estimated to be 2.4 and 1.5 μm, respectively, indicating more frequent cross-slip in 310S SS than 316L SS.

(3) Comparing the results between 310S SS and 316L SS, the susceptibility to SCC is in a good agreement with that of hydrogen embrittlement.

(4) Sensitization heat treatment lowers SCC susceptibility of the steels in hydrogenated water. It is suggested that carbides provide additional hydrogen-trapping site and lowering hydrogen diffusivity, which results in suppression of reaching critical hydrogen content to cause SCC.

References

[1] A.A.F. Tavassoli, Assessment of austenitic stainless steels, Fusion Eng. Des. 29 (1995) 371–390 http://dx.doi.org/10.1016/0920-3796(95)80044-X.

[2] P. Lorenzetto, P. Gierszewski, G. Simbolotti, A European proposal for an ITER water-cooled solid breeder blanket, Fusion Eng. Des. 27 (1995) 423–429, http://dx.doi.org/10.1016/0920-3796(95)90154-X.

[3] P. Lorenzetto, M. Helie, A. Molander, Stress corrosion cracking of AISI 316LN stainless steel in ITER, J. Nucl. Mater. 233–237 (1996) 1387–1392.

[4] V. Belous, G. Kalinin, P. Lorenzetto, S. Velikopolskiy, Assessment of the corrosion behaviour of structural materials in the water coolant of ITER, J. Nucl. Mater. 258–263 (1998) 351–356, http://dx.doi.org/10.1016/S0022-3115(98)00272-4.

[5] D. Tsuru, H. Tanigawa, T. Hirose, K. Mohri, Y. Seki, M. Enoeda, K. Ezato, S. Suzuki, H. Nishi, M. Akiba, Achievements in the development of the water cooled solid breeder test blanket module of Japan to the milestones for installation in ITER, Nucl. Fusion. 49 (2009) 65024, http://dx.doi.org/10.1088/0029-5515/49/6/065024.

[6] Y. Kawamura, H. Tanigawa, T. Hirose, M. Enoeda, S. Sato, K. Ochiai, C. Konno, Y. Edao, T. Hayashi, T. Hoshino, M. Nakamichi, H. Tanigawa, H. Nishi, S. Suzuki, K. Ezato, Y. Seki, T. Yamanishi, Progress of R&D on water cooled ceramic breeder for ITER test blanket system and DEMO, Fusion Eng. Des. 109 (2016) 1637–1643 https://doi.org/10.1016/j.fusengdes.2015.11.002.

[7] K. Arioka, Influence of temperature, hydrogen and boric acid concentration on IGSCC susceptibility of unsensitized 316 stainless steel, J. Inst. Nucl. Saf. Syst. 9 (2002) 116–123.

[8] T. Fukumura, T. Terachi, K. Arioka, Influence of temperature and water chemistry on IGSCC susceptibility of SUS316 in high-temperature water, J. Inst. Nucl. Saf. Syst. 11 (2004) 143–152.

[9] K.J. Choi, S.C. Yoo, H.H. Jin, J. Kwon, M.J. Choi, S.S. Hwang, J.H. Kim, Crack growth behavior of warm-rolled 316L austenitic stainless steel in high-temperature hydrogenated water, J. Nucl. Mater 476 (2016) 243–254, http://dx.doi.org/10.1016/j.jnucmat.2016.04.051.

[10] F. Meng, Z. Lu, T. Shoji, J. Wang, E. hou Han, W. Ke, Stress corrosion cracking of uni-directionally cold worked 316NG stainless steel in simulated PWR primary water with various dissolved hydrogen concentrations, Corros. Sci. 53 (2011) 2558–2565, http://dx.doi.org/10.1016/j.corsci.2011.04.013.

[11] X. Zhong, S.C. Bali, T. Shoji, Effects of dissolved hydrogen and surface condition on the intergranular stress corrosion cracking initiation and short crack growth behavior of non-sensitized 316 stainless steel in simulated PWR primary water, Corros. Sci. 118 (2017) 143–157, http://dx.doi.org/10.1016/j.corsci.2017.02.003.

[12] O. Raquet, E. Herms, F. Vaillant, T. Couvant, J. Boursier, SCC of cold-worked austenitic stainless steels in PWR conditions, 12th Int. Conf. Environ. Degrad. Mater. Nucl. Power Syst. 2005, pp. 1049–1059.

[13] T. Nakagawa, N. Totsuka, T. Terachi, N. Nakajima, Influence of dissolved hydrogen on oxide film and PWSCC of alloy 600 in PWR primary water, J. Nucl. Sci. Technol. 8 (2001) 111–117, http://dx.doi.org/10.1080/18811248.2003.9715330.

[14] J. Chen, Z. Lu, Q. Xiao, X. Ru, G. Han, Z. Chen, B. Zhou, T. Shoji, The effects of cold rolling orientation and water chemistry on stress corrosion cracking behavior of 316L stainless steel in simulated PWR water environments, J. Nucl. Mater. 472 (2016) 1–12, http://dx.doi.org/10.1016/j.jnucmat.2016.01.018.

[15] M. Nono, T. Nakajima, M. Iwama, R. Kasada, A. Kimura, SCC behavior of SUS316L in the high temperature pressurized water environment, J. Nucl. Mater 417 (2011) 878–882, http://dx.doi.org/10.1016/j.jnucmat.2010.12.150.

[16] G.R. Caskey, Hydrogen Compatibility Handbook, (1983), http://dx.doi.org/10.2172/5906050.

[17] G. Han, J. He, S. Fukuyama, K. Yokogawa, Effect of strain-induced martensite on hydrogen environment embrittlement of sensitized austenitic stainless steels at low temperatures, Acta Mater 46 (1998) 4559–4570, http://dx.doi.org/10.1016/S1359-6454(98)00136-0.

[18] L. Zhang, M. Wen, M. Imade, S. Fukuyama, K. Yokogawa, Effect of nickel equivalent on hydrogen gas embrittlement of austenitic stainless steels based on type 316 at low temperatures, Acta Mater 56 (2008) 3414–3421, http://dx.doi.org/10.1016/j.actamat.2008.03.022.

[19] Z. Lu, T. Shoji, Y. Takeda, Y. Ito, A. Kai, N. Tsuchiya, Effects of loading mode and water chemistry on stress corrosion crack growth behavior of 316L HAZ and weld metal materials in high temperature pure water, Corros. Sci. 50 (2008) 625–638, http://dx.doi.org/10.1016/j.corsci.2007.08.021.

[20] Z. Lu, T. Shoji, T. Dan, Y. Qiu, T. Yonezawa, The effect of roll-processing orientation on stress corrosion cracking of warm-rolled 304L stainless steel in oxygenated and deoxygenated high temperature pure water, Corros. Sci. 52 (2010) 2547–2555, http://dx.doi.org/10.1016/J.CORSCI.2010.03.027.

[21] Z. Lu, T. Shoji, F. Meng, Y. Qiu, T. Dan, H. Xue, Effects of water chemistry and loading conditions on stress corrosion cracking of cold-rolled 316NG stainless steel in high temperature water, Corros. Sci. 53 (2011) 247–262, http://dx.doi.org/10.1016/j.corsci.2010.09.018.

[22] Z.P. Lu, T. Shoji, Y. Takeda, Effects of water chemistry on stress corrosion cracking of 316NG weld metals in high temperature water, Corros. Eng. Sci. Technol. 50 (2015) 41–48, http://dx.doi.org/10.1179/1743278214Y.0000000186.

[23] P. Andresen, P. Chou, Effects of hydrogen on SCC growth rate of Ni alloys in BWR water, 15th Int. Conf. Environ. Degrad. Mater. Nucl. Power Syst. - Water React. 2011, pp. 2039–2059.

[24] K. Nakagawa, M. Nono, A. Kimura, Effect of dissolved hydrogen on the SCC susceptibility of SUS316L stainless steel, Mater. Sci. Forum, PRICM7, 2010, pp. 2887–2890, , http://dx.doi.org/10.4028/www.scientific.net/MSF.654-656.2887.

[25] S.M. Bruemmer, J.S. Vetrano, M.B. Toloczko, Microstructure and SCC crack growth of nickel-base alloy 182 weld metal in simulated PWR primary water, 13th Int. Conf. Environ. Degrad. Mater. Nucl. Power Syst. Whistler, British Columbia, 2007, pp. 1–11.

[26] N. Totsuka, Y. Nishikawa, N. Nakajima, Influence of dissolved hydrogen and temperature on primary water stress corrosion cracking of mill annealed alloy 600, Corros 2002 (2002) 1–11.

[27] M. Labousse, D. Déforge, F. Gressier, S. Taunier, M.L.C. Edf, Optimization of the dissolved hydrogen level in pwr to mitigate stress corrosion cracking of nickel alloys. Bibliographic review, modelling and recommandations. Review of experimental results regarding DH effect on initiation and propagation of SCC on, Int. Coop. Gr. Environ. Assist. Crack. 2012, 2012.

[28] T. Yamada, M. Aoki, T. Miyamoto, K. Arioka, SCC growth behavior of cold worked alloy 690 in high-temperature water－Dependence of test temperature, dissolved hydrogen in water, grain boundary carbide and chemical composition－, J. Inst. Nucl. Saf. Syst. 21 (2014) 133–143.

[29] L. Vitos, J.O. Nilsson, B. Johansson, Alloying effects on the stacking fault energy in austenitic stainless steels from first-principles theory, Acta Mater 54 (2006) 3821–3826, http://dx.doi.org/10.1016/j.actamat.2006.04.013.

[30] R.E. Schramm, R.P. Reed, Stacking fault energies of seven commercial austenitic stainless steels, Metall. Trans. A. 6 (1975) 1345–1351, http://dx.doi.org/10.1007/BF02641927.

[31] S. Lu, Q.M. Hu, B. Johansson, L. Vitos, Stacking fault energies of Mn, Co and Nb alloyed austenitic stainless steels, Acta Mater. 59 (2011) 5728–5734, http://dx.doi.org/10.1016/j.actamat.2011.05.049.

[32] C.G. Rhodes, A.W. Thompson, The composition dependence of stacking fault energy in austenitic stainless steels, Metall. Trans. A 8 (1977) 1901–1906, http://dx.doi.org/10.1007/BF02646563.

[33] A. Kimura, H. Kimura, Effect of carbon on the hydrogen induced grain-boundary fracture in iron, J. Jpn. Inst. Met. 47 (1983) 807–813 http://gateway.webofknowledge.com/gateway/Gateway.cgi?GWVersion=2&SrcAuth=mekentosj&SrcApp=Papers&DestLinkType=FullRecord&DestApp=WOS&KeyUT=A1983RV92300001%5Cnpapers3://publication/uuid/010B6DE8-0D77-48CB-930B-15D5FCEB533B.